Spatial interactions modulate tumor growth and immune infiltration

Sadegh Marzban[1], Sonal Srivastava[2], Sharon Kartika[3], Rafael Bravo[1], Rachel Safriel[4], Aidan Zarski[5], Alexander Anderson[1], Christine H. Chung[6], Antonio L. Amelio[2,6], and Jeffrey West[1,*]

[1]Integrated Mathematical Oncology Department, H. Lee Moffitt Cancer Center & Research Institute, Tampa, FL
[2]Department of Tumor Biology, H. Lee Moffitt Cancer Center & Research Institute, Tampa, FL
[3]Department of Biological Sciences, Indian Institute of Science Education and Research Kolkata
[4]Berkeley Preparatory School, Tampa, FL
[5]Greenhill High School, Addison, TX
[6]Department of Head and Neck-Endocrine Oncology, H. Lee Moffitt Cancer Center & Research Institute, Tampa, FL

[*]**jeffrey.west@moffitt.org**

ABSTRACT

Lenia, a cellular automata framework used in artificial life, provides a natural setting to design, implement, and analyze mathematical models of cancer progression and treatment. Lenia's suitability as a cancer model is derived from the strong parallels between artificial life and cancer evolution: morphogenesis, homeostasis, motility, reproduction, growth, stimuli response, evolvability, and adaptation. Historically, agent-based models of cancer progression have been constructed with rules that govern birth, death and migration based on local availability for space, with attempts to map local rules to emergent global growth dynamics. Lenia provides a flexible framework for considering a spectrum of local (cell-scale) to global (tumor-scale) dynamics by defining an interaction kernel governing density-dependent growth dynamics. First, we show Lenia can recapitulate a range of cancer model classifications including local or global, deterministic or stochastic, non-spatial or spatial, single or multi-population, and off or on-lattice. Lenia is subsequently used to develop data-informed models of 1) single-population growth dynamics, 2) multi-population cell-cell competition models, and 3) cell migration or chemotaxis.

1 Introduction

LENIA (from the Latin *lenis* meaning "smooth") is a cellular automata framework that allows for continuous space and time. Cellular automata are often used to study the "rules" that can recapitulate the collective behavior of interacting biological "agents" (e.g. individual cells or organisms). The development of Lenia was spurred by the search for rule-sets that lead to features that are important in artificial life: self-organization (morphogenesis) self-regulation (homeostasis), self-direction (motility), self-replication (reproduction), growth (development), response to stimuli or environmental factors, evolvability, adaptation[1,2], and other emergent complexity[3].

Many of these same features (e.g. cellular replication, growth, motility, evolvability, and adaptation) are important in the development of complex, multi-factorial diseases such as cancer. Thus, the purpose of this manuscript is to extend the Lenia framework as a tumor model, including immune predation and escape. We show how this is a natural extension, as Lenia has the capability to recapitulate 1) classical analytical models of cancer (ordinary differential equations), 2) common stochastic agent-based models of cancer, 3) standard models of multiple cell types competing on a Darwinian fitness landscapes (evolutionary game theory), and 4) generalized cell migration (e.g. chemotaxis models) common in cancer mathematical

modeling literature.

1.1 The overlap in modeling artificial life and cancer evolution

In its original formulation, Lenia defines an on-lattice domain where each grid location can take a continuous value of density. Methods of interactive evolutionary computation were used to find rule-sets that lead to defined, artificial "creatures" (see figure 1A for examples) which are capable of stable linear or angular motion or other life-like characteristics (figure 1B)[1,2]. These continuous creatures are reminiscent of the binary gliders, oscillators, and still-life creatures in Conway's Game of Life[4].

Grid locations change according to an update rule describing the growth dynamics (figure 1C) paired with an interaction kernel function (figure 1D). For example, tumor cell density in a two-dimensional domain (figure 1E) is convolved with an interaction kernel (figure 1F) to calculate the "density potential" (figure 1G). Density potential is the surrounding density of grid locations weighted by kernel interaction function of radial distance from the focal cell. This defines a spatially-explicit growth field (figure 1H)[1], whereby the update rule is enacted iteratively at each time step, t (figure 1I). Thus, a natural interpretation of Lenia as a cancer model is a spatial density map of cancer cells. Cancer cells grow according to a local density-dependent growth rate (e.g. logistic growth) which is a function of local cell density. Lenia can compare the effect of local (short-range kernels) versus global (long-range kernels) on growth dynamics.

There exists broad overlap in both methods and desired emergent behavior between models of artificial life and models of cancer growth (figure 1H). To adequately mimic biological realism in cancer, mathematical frameworks have implemented methods classified as 1) non-spatial or spatial, 2) deterministic or stochastic, and 3) single or multiple populations (cell types). Lenia allows for flexible model design to incorporate the full range of these classifications. Extensions to Lenia include Glaberish (a variant that leads to pattern formations that are stable in space or time[5]), Flow-Lenia (imposes mass conservation over time)[6], Asymptotic-Lenia (asymptotic, smooth updating)[7], Particle-Lenia (off-lattice)[8], or a generalized reaction-diffusion implementation[9].

1.2 Modeling spatial effects in tumor-immune dynamics

Spatio-temporal models of cancer growth dynamics

Tumor growth can be expressed as a mathematical law using an ordinary differential equation (ODE)[10] and used as a predictive tool in assessing the course of tumor progression[11,12]. ODE frameworks use the well-mixed assumption, where each cell is equally likely to interact with each other cell in the tumor. Thus, there is a broad interest in understanding the effect of local, cell-scale contact inhibition on the emergent tumor-scale global growth dynamics[13,14]. The choice of spatial structure within a model (e.g. non-spatial, deme models, mesoscale, or boundary-driven growth) affects the evolutionary dynamics within heterogeneous tumors[15–17], tumor growth dynamics[18,19] and the emergent pattern formation[20–22].

Lenia is classified as a system of integro-differential equations (IDE)[23]. IDEs have been used to study cancer progression[24] and treatment[25] or to find approximations of stochastic ABMs in cancer[26], but these formulations often focus on how interaction kernels alter the time scale of dynamics or the system stability. Lenia provides a unifying framework for direct comparison of well-mixed assumptions commonly used in ODE models (corresponding to Lenia's long-range kernel) and local-scale competition commonly used in stochastic agent-based modeling (corresponding to Lenia's short-range kernels).

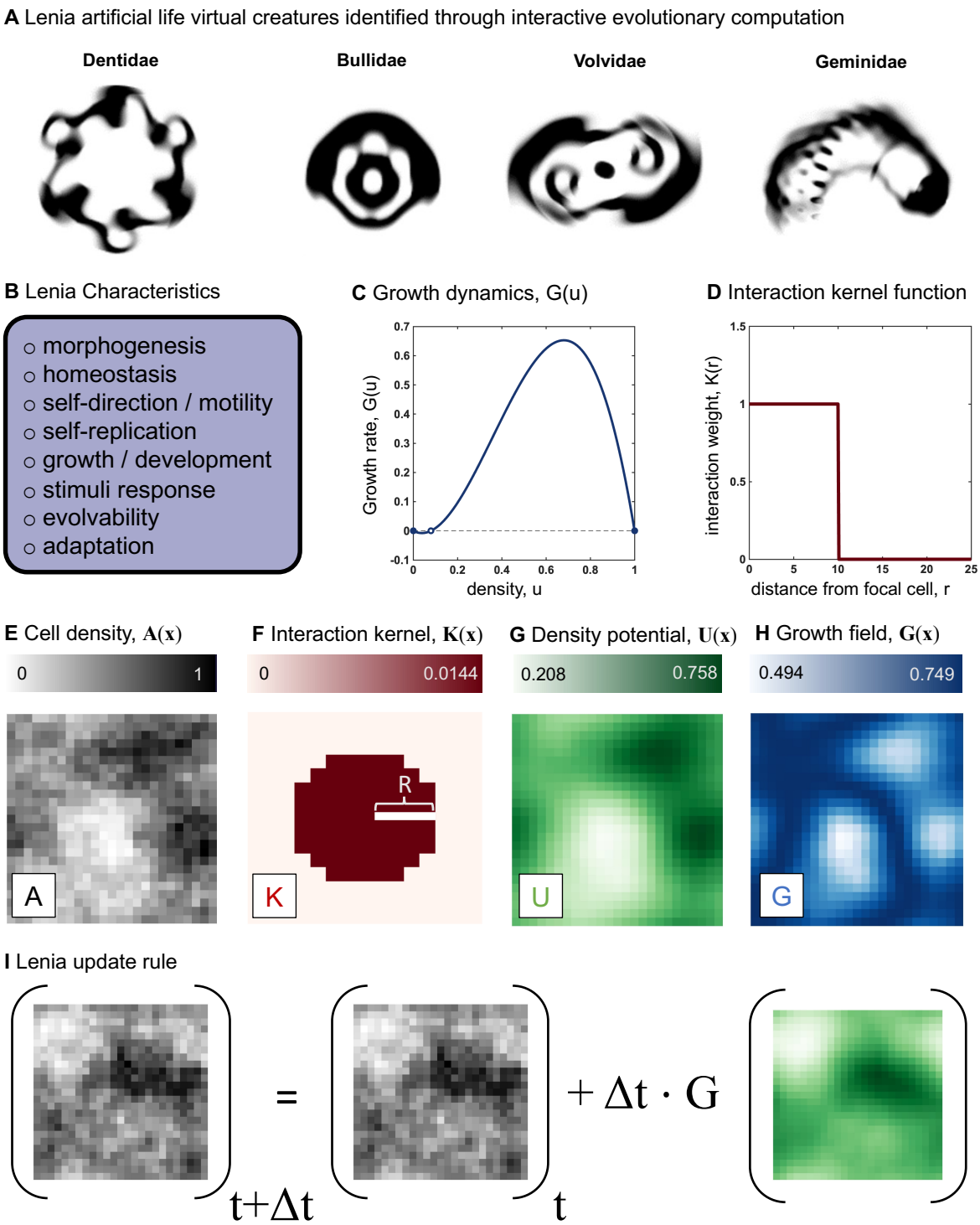

Figure 1. Lenia as a cancer model: (A) Lenia artificial life virtual creatures, reproduced from ref. 1. (B) List of characteristics possible to produce in Lenia by varying the growth dynamics function (C) or the interaction kernel function (D). (E) An example snapshot of a simulation shows the density of cells at each lattice location where the interaction kernel (F) specifies the nature of interaction of cells depending on their distance from each other. (G) The density potential, interpreted as a weighted average of interactions at each lattice location, is calculated as the convolution of $\mathbf{A}(\mathbf{x})$ and $\mathbf{K}(\mathbf{x})$. (H) the growth field calculated by applying a growth map to the density potential. (I) adding a fraction of the growth field at each time step to the cell density, forms the Lenia update rule, as seen in eqn. 1.

Spatio-temporal models of tumor-immune interactions

Tumors do not grow in isolation but must develop immune escape mechanisms to avoid extinction. Tumor-immune interactions have been described using logistic tumor growth with immune recruitment and exhaustion (e.g. ref. 27) or as a predator-prey relationship (e.g. ref. 28).

Importantly, the predator-prey relationship may be insufficient to describe tumor-immune dynamics without also considering mechanisms for avoiding oscillatory behavior common to these models[29]. Thus, in the models developed herein we include Allee effects, whereby tumors require a cooperative benefit of close aggregation when at lower densities[30]. Allee effects lead to a decreased growth benefit when tumor density is low, and thus proposed to enable immune predation to fully eliminate tumors in the absence of immune escape[29].

Immune predation has likewise been modelled using integro-differential equations[31–34], mesoscopic models[35], or stochastic agent-based methods[36].

Spatio-temporal models of cell migration and the extracellular matrix

The migration of cancer cells is influenced by the spatial configuration of collagen as they navigate through preexisting spaces[37]. The extracellular matrix (ECM), particularly the density and orientation of collagen fibers, can also influence migration through contact guidance, thereby facilitating both migration and invasion[38]. It is essential to understand the process of cancer cell metastasis, particularly in terms of how cancer cells reach the bloodstream and migrate through the extracellular matrix (ECM), as explored in this paper[39]. The study investigates the impact of collagen, a key component of the ECM, focusing on its orientation and thickness, on the migration of cancer cells away from their original location[39].

In summary, stochastic birth-death-migration models are commonly used to model tumor growth dynamics, often with a focus on deriving approximations that map local interaction dynamics to global mean-field approximations. Alterations in cell migration, proliferation, and death parameters may lead to spatial heterogeneity in cell density, reducing the accuracy of naive mean-field approximations. Thus, it's convenient for a cancer modeling framework to include 1) non-spatial or spatial, 2) deterministic or stochastic, and 3) single or multiple populations (cell types). Below, we illustrate how the Lenia mathematical framework integrates each of these components. Next, we illustrate how classical growth dynamics models (e.g. logistic growth) are a special case of Lenia. Then, we illustrate how multi-channel Lenia can be used to model cell-cell (tumor-immune) interactions. Finally, we show particle Lenia as an example of immune cell trafficking in cancer.

2 Results

2.1 Increased range of interaction increases tumor diffusivity and speeds growth

First, we implement a single population (one cell type) model of tumor growth dynamics in figure 2. Growth dynamics are described by logistic growth with an Allee threshold (eqn. 4), such that tumors are seeded above the Allee threshold have positive growth. The solution to this ordinary differential equation is shown in blue in figure 2A. Comparing deterministic Lenia (figure 2A; solid lines) illustrates that systematically reducing the effective range of the interaction kernel reduces the rate of growth, and alters the temporal dynamics. Smaller interaction kernels (e.g. black lines) are characterized by slow growth due to the presence of contact inhibition in small interaction neighborhoods.

Reduction in kernel size also alters the spatial variegation of tumor density. For example, short-range kernels (figure 2B, left) are characterized by sharp, well-defined boundary drive growth while long-range

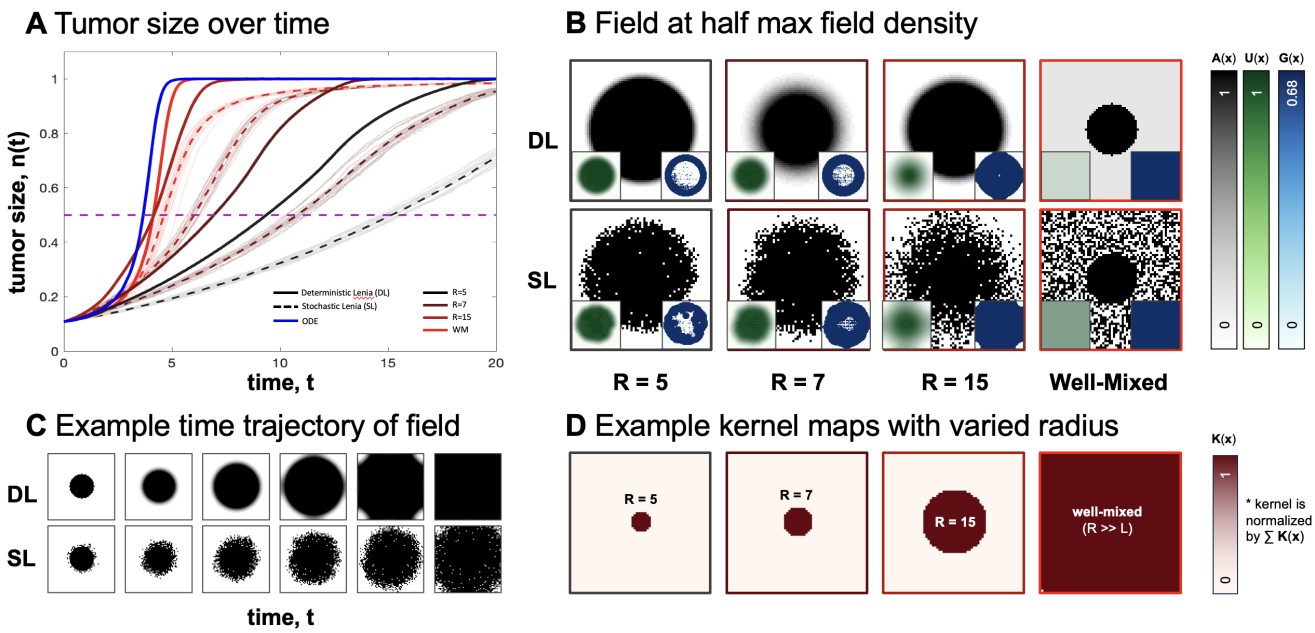

Figure 2. Cancer growth dynamics in Lenia (A) Average cell density over time for varying kernel sizes, for deterministic and stochastic lenia. Averages over stochastic runs are shown in dotted lines and individual trajectories are shown in translucent lines. ODE solution (shown in blue) matches simulation with a well-mixed kernel. (B) State of field at half maximal capacity for different kernel sizes for stochastic and deterministic Lenia. Density potential and Growth distribution shown in inset. (D) State of field at progressive time points for kernel size 4 for deterministic and stochastic Lenia. (E) Kernels used in models in figures (B).

kernels (figure 2B, right) are associated with diffuse patterns.

This pattern holds when considering either a deterministic (figure 2B; DL) or a stochastic (figure 2B; SL) update rule (see Supplemental section S1.1). The average of many stochastic realizations is shown in dashed lines (figure 2A), which tend to underestimate the deterministic simulation with the corresponding kernel size. This is due in part to the fact that the cell density map $\mathbf{A}(\mathbf{x})$ in stochastic Lenia is restricted to integer values only (compare figure 2D, where only values of 0 or 1 are allowable in stochastic Lenia). These results illustrate the utility of Lenia to interpolate between two standard modeling approaches: 1) ordinary differential equations and 2) stochastic, local agent-based methods. Lenia extends standard methods to allow investigation of arbitrary interaction kernels.

2.2 Short-range interaction kernels are more robust to Allee effects

Next, we investigate the interplay between the Allee threshold and the interaction kernel. Logistic growth with an Allee threshold has an unstable equilibrium which drives the population to extinction when tumor density is below the threshold. As shown in figure 3A, simulating logistic growth with Allee in an ODE (blue line) or a well-mixed (red line; WM) both result in eventual extinction. Interestingly, reducing the interaction kernel distance, R, results in positive tumor growth (e.g. black line). This effect occurs for a range of Allee threshold values and kernel sizes, shown in figure 3B. This clearly illustrates an expanded region of positive growth when kernel size is low, across a wide range of threshold values. Smaller neighborhoods increase the likelihood that a single cell's neighborhood will maintain a sufficient density above the Allee threshold, and thus maintain positive growth.

While stochastic Lenia is typically associated with slower temporal scales (figure 3A, dashed lines), the long-term tumor fate (extinction or growth) are analogous in both models and spatial variegation patterns

are also similar (figure 3C,D). These results suggest that well-mixed model formulation may overestimate the role of an Allee effect (thus overestimating the likelihood tumor extinction). In the next section, we investigate the effect of interaction kernel size on immune predation of tumors.

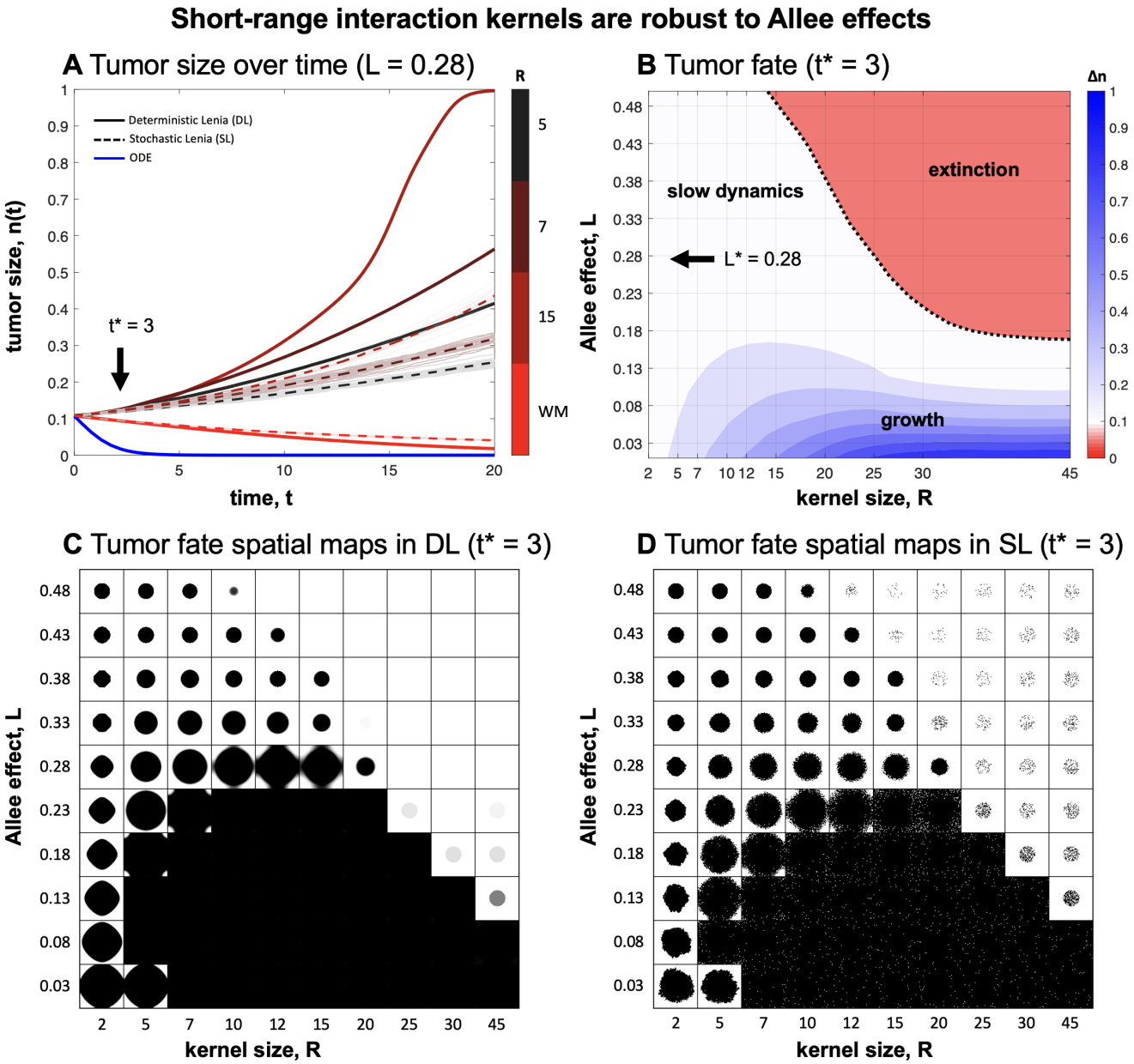

Figure 3. Short-range interaction kernels are more robust to Allee effects (A) Average cell density over time for varying kernel sizes, for deterministic and stochastic Lenia. Averages over stochastic runs are shown in dotted lines and individual trajectories are shown in translucent lines. ODE solution shown in blue. (B) Long-term tumor fate for deterministic Lenia where trajectories that eventually result in extinction are shown in red, or growth shown in blue (colorbar indicates change in tumor size at $t^* = 3$. (C, D) Spatial maps shown for deterministic Lenia (C) and stochastic Lenia (D) at time $t^* = 3$.

2.3 High immune specificity and sensitivity maximize tumor regression

In order to investigate the effect of short-range and long-range interactions between tumor and immune cells, we employ the multi-channel Lenia model to simulate the dynamics of in a tumor-immune (figure

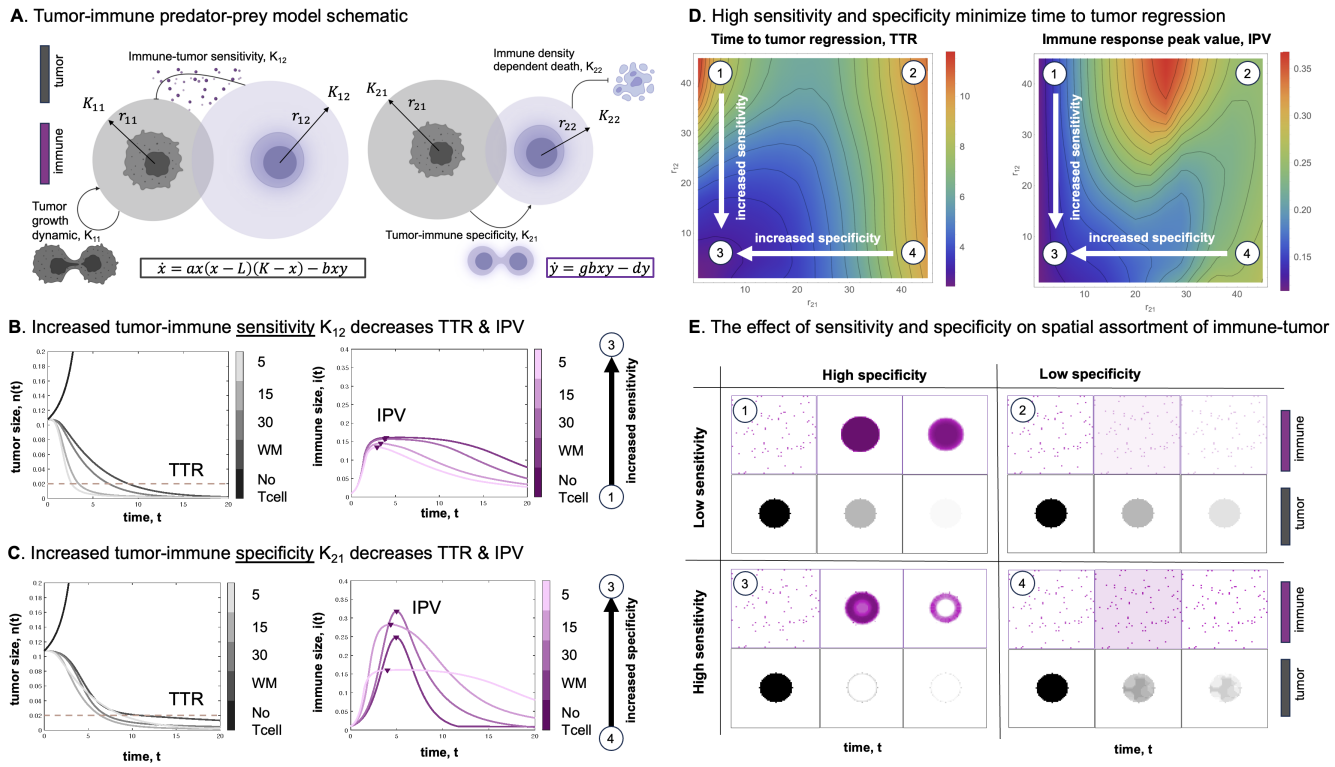

Figure 4. Competition dynamics in Lenia (A) Schematic representation of the tumor-immune predator-prey model, illustrating various kernel sizes for tumor growth (K_{11}), predation distance (K_{12}), immune recruitment (K_{21}), and density-dependent death distance in the immune system (K_{22}). **(B)** Impact of different predation distances (K_{12}) and immune recruitment (K_{21}) on the integration results of the tumor-immune predator-prey model, with other kernels held well-mixed. **(C)** Spatial outcomes of the tumor and immune response in the model, showcasing the influence of different kernel sizes. **(D)** Effect of varying predation and recruitment (K_{12} and K_{21}) on the time to tumor regression (considered when there are 2% tumor cells in the area) and the peak value in the immune response.

4). Tumor-immune dynamics are described by the predator-prey model in eqns. 6 and 7. Similar to the previous figure, this model contains an Allee threshold whereby tumor cells are driven to extinction below this threshold even in the absence of immune cells[29].

As seen in schematic figure 4A, there are four interaction kernels: tumor-tumor, tumor-immune, immune-tumor, and immune-immune. We define the tumor-immune kernel (K_{12}) as the **immune sensitivity**, whereby a short-range K_{12} is characterized by an increase in immune kill rate and decreasing the time to tumor regression (TTR) as seen in figure 4B. Next, we define the immune-tumor kernel as the **immune specificity**, whereby a short-range K_{21} leads to more rapid recruitment of immune cells, resulting in high immune peak value, IPV (see figure 4C). A reduction in the recruitment distance (small K_{21}) leads to the production of an immune response in closer proximity to tumor cells (refer to figure 4E). Similarly, decreasing the predation distance (K_{12}) causes the immune response to impact the tumor locally.

As seen in figure 4D, both immune specificity and immune sensitivity are required to maximize tumor regression. This effect is illustrated by observing spatial maps over time in figure 4E. High specificity results in rapid recruitment concentrated within the tumor, but these immune cells are most effective at removing tumor when sensitivity is high (case 3). In contrast, low specificity results in a diffuse spatial pattern of immune recruitment through the domain, where most immune cells are not co-localized with tumor cells, effectively wasting a majority of immune response (cases 2 and 4). Consequently, immune cells that do infiltrate tumor are rare but strongly effective, leading to a heterogeneous tumor kill (case 4).

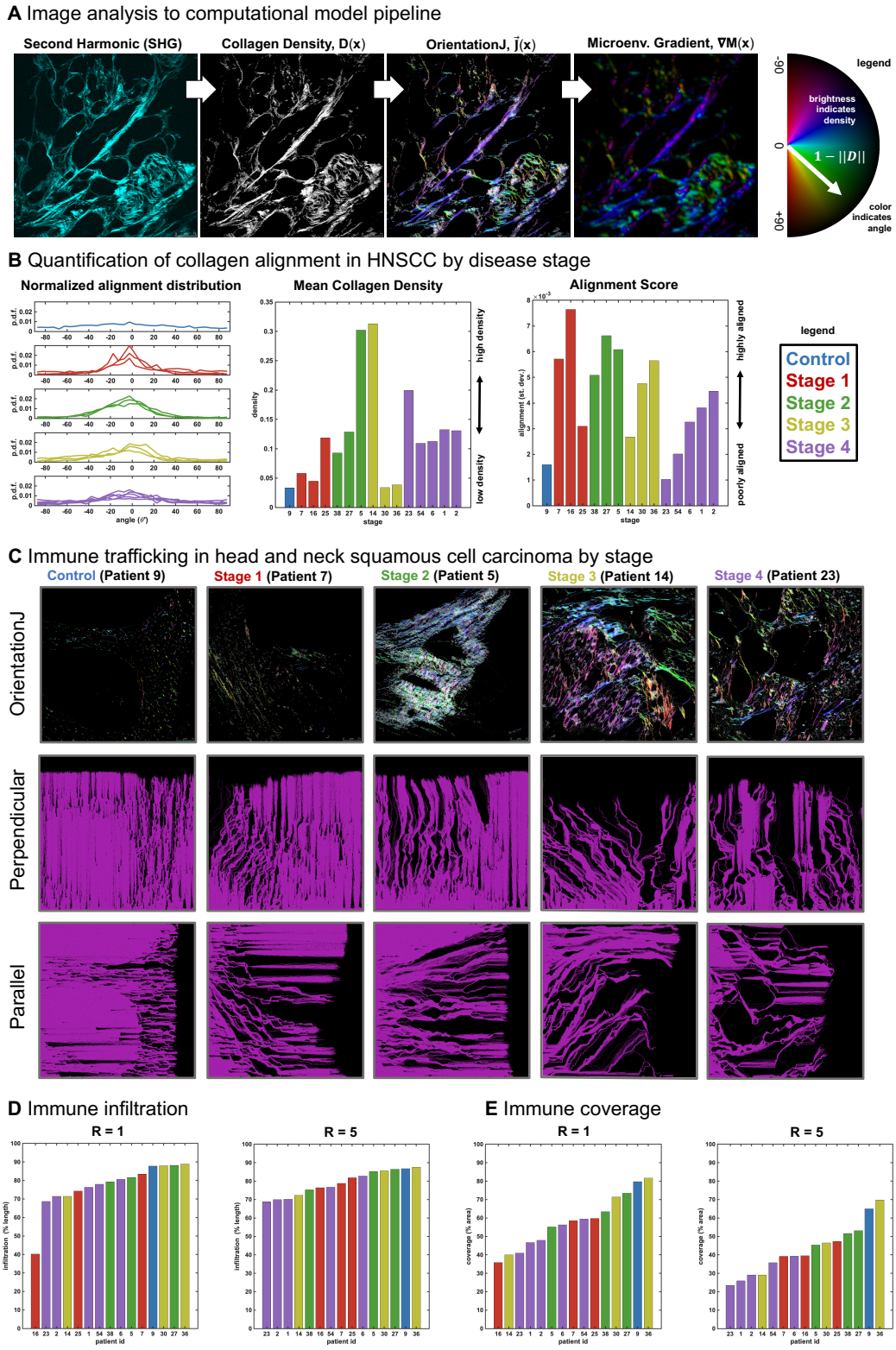

Figure 5. Immune cell trafficking model in Particle Lenia (A) Pipeline of image analysis to computational model using second harmonic generation to determine collagen density and subsequently the alignment and microenvironmental gradient.(B) Alignment and density of collagen fibers is determined using OrientationJ ImageJ plugin[40], colored by disease stage. (C) Representative sample simulated data by disease stage (columns), showing the original alignment image (top) and simulated for perpendicular (middle) and parallel (bottom) models. (D, E) Immune infiltration (D) and immune coverage (E) ordered sequentially and colored by stage, repeated for two kernel sizes ($R = 1, 5$).

2.4 Collagen structure alignment predicts poor immune infiltration in squamous cell carcinomas

Next, we illustrate an example of a cell migration model using an extension of Particle Lenia. In figure 5A, we introduce an immune cell trafficking model where each simulated immune cell moves along a microenvironment gradient field determined by collagen fiber alignment (eqn. 8). Late-stage head and neck squamous cell carcinomas (HNSCC) are associated with increased deposition and alignment of fibrillar collagens[41]. We hypothesize that poor outcomes are partially due to poor immune cell infiltration caused by deposition of a dense collagen barrier.

The pipeline of model development is shown in figure 5A. Second harmonic generation (SHG) is performed on a cohort of squamous cell carcinomas to quantify collagen density. Each patient has a selected region of interest (ROI) to perform SHG, and are subsequently analyzed using OrientationJ ImageJ plugin to determine alignment[40]. Each pixel is color-coded according to the directionality of collagen fibers, such that fibers aligned in a single direction are colored with the same hue on the red-blue-green-yellow spectrum (figure 5A, semi-circle legend color-bar). The microenvironment gradient field, $\partial\mathbf{M}(\mathbf{x})$ at each grid location $\mathbf{x}$ is determined by the convolution of interaction kernel and the OrientationJ vector field, weighted by collagen density (see Methods). Thus, immune cells move in the same direction as collagen fiber alignment.

Imaging data are quantified in figure 5B, which illustrates the correlation of disease stage with collagen density and alignment. Normal adjacent control tissue and early stage HNSCC's are associated with sparse and heterogeneous collagen alignment, while late-stage HNSCC tends to contain highly aligned collagen fiber patches. We hypothesized that late-stage disease is associated with collagen structures which lead to poor immune infiltration. Next employ Lenia to test two plausible cell migration models describing the movement of immune cells in response to collagen: parallel or perpendicular movement.

Model simulations are shown in figure 5C for a model seeded with corresponding collagen ROI (top row). Immune cells are seeded along one edge of the domain ($N = 5$ cells per pixel) and simulated for T timesteps. Typically, as disease stage increases (figure 5C, left to right), immune cell infiltration and coverage decrease (purple area indicates the portion of the domain which at least one immune cell has trafficked). Well-aligned collagen structures result in a strongly directed migration, deviating immune cells from providing a well-mixed coverage of the domain.

In simulations, the total time is chosen such that immune cells in an empty domain would migrate in a linear, unaltered fashion and provide 100% infiltration and 100% coverage of the domain. In this way, we define infiltration as the fraction of the domain length traveled. Average infiltration across all immune cells is shown in figure 5D, illustrating a patient-specific infiltration prediction. We note that stage 4 disease (purple bars) is typically associated with poor infiltration while the control (blue bar) is associated high infiltration. Finally, in figure 5E, we plot immune coverage: the fraction of the domain area which is covered by at least one immune cell. The analysis is repeated for two interaction kernel sizes ($R = 1, 5$), leading to minor differences in trends.

3 Methods

3.1 Lenia Cellular Automata

The notation here follows ref. 1, which we re-state here for clarity. Lenia is a cellular automata defined by five components: 1) a discrete grid of points, $\mathscr{L}$, (herein we consider two-dimensional lattice grid $\mathscr{L} \in \mathbb{R}^2$), 2) the range of allowable states $\mathscr{S} = [A_{\texttt{min}}, A_{\texttt{max}}]$, 3) the local update rule $\phi : \mathscr{S}^{\mathscr{N}} \to \mathscr{S}$ is the local update rule, 4) the neighborhood around each focal cell at location $\mathbf{x}$, given by $\mathscr{N}_{\mathbf{x}} = \{\mathbf{x}+\mathbf{n} : \mathbf{n} \in \mathscr{N}\}$, and 5) time steps $t \in \mathscr{T}$. The spatial *cell density* map configuration is defined by $\mathbf{A}^t : \mathscr{L} \to \mathscr{S}$: the collection of states over the whole grid, at time $t \in \mathscr{T}$, the timeline. Herein, we let $\mathbf{A}$ be a two-dimensional matrix where $\mathbf{A}(\mathbf{x})$ represents the cell density at grid location $\mathbf{x}$ which is updated via the following equation:

$$\mathbf{A}^{t+\Delta t}(\mathbf{x}) = \Big[\mathbf{A}^t(\mathbf{x}) + G(\mathbf{U}^t(\mathbf{x}))\Delta t\Big]_{A_{\texttt{min}}}^{A_{\texttt{max}}} \tag{1}$$

where $G(u)$ is the density-dependent growth function defined on the interval $u \in [A_{\texttt{min}}, A_{\texttt{max}}]$. For each point $\mathbf{x}$, the convolution of a kernel $\mathbf{K}$ with $\mathbf{A}^t(\mathscr{N}_{\mathbf{x}})$ is calculated to compute the potential distribution $\mathbf{U}^t$:

$$\mathbf{U}^t(\mathbf{x}) = \mathbf{K} * \mathbf{A}^t(\mathbf{x}) = \sum_{\mathbf{n} \in \mathscr{N}} \mathbf{K}(\mathbf{n}) \cdot \mathbf{A}^t(\mathbf{x}+\mathbf{n}) \tag{2}$$

Thus, the growth is defined at every lattice location: $\mathbf{G}^t(\mathbf{x}) := G(\mathbf{U}^t(\mathbf{x}))$. A fraction of the growth distribution is added to each site at each time step (Euler approximation update rule) and the value at the site is clipped to $[A_{\texttt{min}}, A_{\texttt{max}}]$.

3.2 Interpretation of Lenia as a cancer model

Next, we make explicit the connection to cancer modeling. Lenia provides a natural framework for constructing mathematical models of cancer cell growth, competition, and migration, where each lattice location $\mathbf{x}$ contains a density of tumor cells, $\mathbf{A}^t(\mathbf{x})$. When modeling tumor dynamics, set $A_{\texttt{min}} = 0$ and $A_{\texttt{max}} = C$ where C represents the maximum resource- or space-limited carrying capacity of cells within each single lattice location. Classic cell interaction neighborhoods such as von Neumann (the four nearest neighbors; $R = 1$) or Moore (eight nearest neighbors; $R = 1.8$) can be written as an interaction kernel function, defined as a circle of radius R:

$$K(r) = \varepsilon \cdot (1 - H(R - r)) \tag{3}$$

where H is the Heaviside function, and ε is chosen to normalize the elements of the kernel to sum to one. Thus, $\mathbf{U}(\mathbf{x})$ represents a potential density that is perceived by the focal location, determining the location-specific growth rate of cells, $G(\mathbf{U}(\mathbf{x}))$. The density potential is the convolution of cell density within the neighborhood, $\mathbf{A}(\mathscr{N}_x)$, weighted (convolved) by the values in the kernel function. Typical kernel functions in cancer modeling are likely to be non-increasing functions of the radial distance from the focal location. For notational convenience, define the mean density of the field as $\hat{n}(t) = \frac{1}{||\mathscr{L}||}\sum_{\mathbf{x}\in\mathscr{L}} \mathbf{A}^t(\mathbf{x})$, where $||\mathscr{L}||$ is the total number of lattice locations in domain $\mathscr{L}$.

Lenia can be extended to a stochastic setting by restricting only integer values on each lattice point ($\mathbf{A}(\mathbf{x}) \in [0, 1, 2, \ldots, A_{\texttt{max}}]$) with stochastic updates (see Supplemental Section S1.1). We note that classic

agent-based methods often restrict each lattice location to contain at most a single cell ($A_{\texttt{max}} = 1$) and make the implicit assumption that cells divide into surrounding empty locations with probability b. This is qualitatively similar to defining a Moore-like or von Neumann-like interaction kernel with $G(\mathbf{U}(\mathbf{x})) = b$.

3.2.1 Tumor growth dynamics model

We first model tumor growth as a local logistic growth dynamic, shown in figure 1E, and F given by:

$$G(u) = \gamma u(C-u)(u-L) \tag{4}$$

where γ is the intrinsic growth rate of tumor cells, C is the carrying capacity (maximum density) of each lattice location, L is the allee effect, and u is the density potential (eqn. 2).

3.2.2 Tumor-immune predator-prey model

Using multi-channel Lenia, we can extend the model to account for cell density of multiple cell types, $\mathbf{A}_i(\mathbf{x})$ where $i \in \{1,2,\ldots,N\}$. For example, herein we consider competition between $N = 2$ cell types that each have a growth field which is a function of the density potential for both cell types: $\mathbf{G}_i^t(\mathbf{x}) := G_i(\mathbf{U}_1^t(\mathbf{x}), \mathbf{U}_2^t(\mathbf{x}))$. In this two-type case, the dynamics are given by:

$$\mathbf{A}_i^{t+\Delta t} = \left[\mathbf{A}_i^t + G_i\left(\mathbf{U}_{i1}^t(\mathbf{x}), \mathbf{U}_{i2}^t(\mathbf{x})\right)\Delta t\right]_{A_{i,\texttt{min}}}^{A_{i,\texttt{max}}} \tag{5}$$

Thus, the tumor-immune model can be written:

$$\underbrace{G_1(u_{11},u_{12})}_{\texttt{tumor (prey)}} = \underbrace{\gamma u_{11}(u_{11}-L)(C-u_{11})}_{\texttt{logistic growth with Allee}} - \underbrace{bu_{11}u_{12}}_{\texttt{predation}} \tag{6}$$

$$\underbrace{G_2(u_{21},u_{22})}_{\texttt{immune (predator)}} = \underbrace{g(bu_{21}u_{22})}_{\texttt{predator growth}} - \underbrace{du_{22}}_{\texttt{natural death}} \tag{7}$$

where u_{ij} represents the density of cell type j perceived by cell type i. The Allee threshold is given by L, carrying capacity of tumor cells is C, and predation rate is b. Immune cells and expand at rate g (weighted by immune predation response) and die at rate d.

Modeling cell migration using Particle Lenia

A recent extension referred to as Particle Lenia extends the mathematical framework to off-lattice. The location of each cell i is given by vector $\mathbf{p}_i := \{x,y\}$ corresponding to its location in two-dimensions. Movement of the particle is determined by the local gradients of the energy and chemotactic migration fields: $\mathbf{E}(\mathbf{p}_i)$ and $\mathbf{M}(\mathbf{p}_i)$, respectively.

$$\frac{d\mathbf{p}_i}{dt} = \underbrace{-\nabla\mathbf{E}(\mathbf{p}_i)}_{\texttt{cell adhesion-repulsion}} + \underbrace{\nabla\mathbf{M}(\mathbf{p}_i)}_{\texttt{microenvironment}} = -\frac{\partial\mathbf{E}(\mathbf{p}_i)}{\partial(\mathbf{p}_i)} + \frac{\partial\mathbf{M}(\mathbf{p}_i)}{\partial(\mathbf{p}_i)} \tag{8}$$

Particles (i.e. cells) in this model move against the local gradient of the energy field, representing particle interactions[a]. The cell-cell repulsion and adhesion fields are a function of the potential field, $\mathbf{E}^t(\mathbf{x}) = E(\mathbf{U}^t(\mathbf{x}))$ (see Supplemental info section S1.2). Similarly, an extrinsic microenvironmental field $\mathbf{M}(\mathbf{p}_i)$, defines the chemotactic direction of cells moving toward a nutrient-based or bio-mechanical gradient. The cell position update rule can be deterministic (following the highest point of gradient) or stochastic (weighted in the direction of gradient).

Modeling the effect of collagen on T-cell migration

In this manuscript, we assume negligible T-cell adhesive-repulsive interactions such that $E(\mathbf{U}^t(\mathbf{x})) = 0$. Instead, T-cells move in a directed fashion influenced by the surrounding extrinsic microenvironment according to the following equation:

$$\nabla \mathbf{M}(\mathbf{p}_i) \quad = \quad \mathbf{K} * \vec{\mathbf{C}}^t(\mathbf{x}) \tag{9}$$

where $\mathbf{K}$ is the cell-microenvironment interaction kernel (see eqn. 3), $\vec{\mathbf{C}} = \{||C||, \theta\}$ is a vector field determined by collagen fiber alignment. At each time point, noise is added to the collagen vector field's angle such that $\theta' = \theta + R(\sigma)$ where R is a uniform random variable on $[0, \sigma]$ radians.

In this way, we model the influence of collagen fibers to direct T-cell movement as a weighted vector summation of the collagen fiber alignment in the focal T-cell's local neighborhood. The collagen fiber alignment vector field is inversely proportional to the density of collagen (cells travel slowly in dense fibers). We consider two plausible models of the influence of collagen on T-cell migration: T-cells travel 1) in parallel to collagen fibers or 2) perpendicular to collagen fibers, denoted $\|$ and $\perp$, respectively.

$$\vec{\mathbf{C}}(\mathbf{x}) \quad = \quad (1 - \mathbf{D}(\mathbf{x}))\vec{\mathbf{J}}_{\perp}(\mathbf{x}) \tag{10}$$

$$\vec{\mathbf{C}}(\mathbf{x}) \quad = \quad (1 - \mathbf{D}(\mathbf{x}))\vec{\mathbf{J}}_{\|}(\mathbf{x}) \tag{11}$$

where $\vec{\mathbf{J}}(\mathbf{x})$ is collagen fiber alignment (a unit vector) derived from clinical imaging, detailed in the next section below, scaled by the inverse of the normalized density of collagen at each grid location, $\mathbf{D}(\mathbf{x}) \in [0, 1]$.

Immune cell migration field defined using OrientationJ

Tumor microarray (TMA) having FFPE tissue samples from HPV-negative HNSCC patient cohort from the H. Lee Moffitt Cancer Center and Research Institute (IRB: MCC#18754) was analyzed to determine collagen alignment in the tumor microenvironment. The TMA cores were imaged using a Leica SP5 AOBS multiphoton confocal microscope and a 25x, HC IR Apo, NA 0.95 water immersion objective. The excitation wavelength was tuned to 880 nm and emitted light was detected at 440 nm using bandpass filters for detecting the SHG signal of collagen. The SHG images were analyzed using the Orientation J plugin[40] in ImageJ software which provides both visual and quantitative data outputs for collagen fiber alignment[43].

[a]For example, one might define $\mathbf{E}$ as the Lennard-Jones potential function, which describes the balance of repulsive and attractive forces as a function of the distance between two interacting particles[42]

4 Discussion

Lenia demonstrates the capability to recapitulate important features required for modeling the evolution and ecology of cancer. While here we focus here on modeling tumor-immune spatial interactions, the role of spatial structure more broadly has important implications for optimizing cancer treatment[44,45], modulating evolutionary dynamics of tumor heterogeneity[15,17,46], and altering cell-cell competitive dynamics[47] even when using the same interaction rules[48,49]. Lenia is flexible enough to mimic non-spatial (well-mixed) ordinary differential equations (with sufficiently large kernel sizes) as well as small-scale spatial neighborhoods commonly used in agent-based methods, such as Moore or von Neumann neighborhoods. It is also straightforward to simulate deterministic dynamics and the corresponding stochastic dynamics. Additionally, Lenia can simulate ecological interactions between multiple cell types in heterogeneous tumors. We have shown the ability of Lenia to recapitulate common models of tumor-immune dynamics (logistic-Allee and Lotka-Volterra). Finally, we illustrate the ability of Particle Lenia to recapitulate cell migration and trafficking in an off-lattice, with a schematic example in squamous cell carcinomas. However, Lenia provides several natural advantages over traditional birth-death-migration models. Kernel convolution can be performed using fast-Fourier transforms, drastically decreasing the computational cost of simulations. Additionally, convolution of extrinsic migration gradient can be pre-computed, increasing computational efficiency.

S1 Supplemental Information

S1.1 Stochastic Lenia

The Lenia framework can be extended to a stochastic setting by considering the likelihood of a lattice location $\mathbf{x}$ containing a single cell. Let $\mathbf{A}(\mathbf{x}) \in [0,1]$ be a random variable, such that the probability, P, of a cell potentially being added to an existing lattice location $\mathbf{x}$ at the next time step $t + \Delta t$. This probability is determined by the Binomial distribution (if the lattice location is currently empty), at a rate of $G(\mathbf{U}(\mathbf{x}))\Delta t$.

S1.2 Particle Lenia

Particle Lenia is an extension of Lenia where movement of the particle is determined by the sum of two local gradients representing the energy field, $\mathbf{E}(\mathbf{p}_i)$, and migration field, $\mathbf{M}(\mathbf{p}_i)$. Particle i's location in two-dimensional space is given by $\mathbf{p}_i := \{x, y\}$ and updated according to the following equation:

$$\frac{d\mathbf{p}_i}{dt} = \underbrace{-\nabla\mathbf{E}(\mathbf{p}_i)}_{\texttt{cell adhesion-repulsion}} + \underbrace{\nabla\mathbf{M}(\mathbf{p}_i)}_{\texttt{microenvironment}} = -\frac{\partial\mathbf{E}(\mathbf{p}_i)}{\partial(\mathbf{p}_i)} + \frac{\partial\mathbf{M}(\mathbf{p}_i)}{\partial(\mathbf{p}_i)} \tag{12}$$

Particles (or cells) move against the local gradient of $\mathbf{E}(\mathbf{x})$, the energy field. The cell-cell repulsion and adhesion fields are a function of the potential field, $\mathbf{U}$, such that:

$$\mathbf{E}^t(\mathbf{x}) = E\left(\mathbf{U}^t(\mathbf{x})\right) \tag{13}$$

$$= E\left(\textstyle\sum_i \mathbf{K}\left(\mathbf{x} - \mathbf{p}_i^t\right)\right) \tag{14}$$

$$= E\left(\textstyle\sum_i K\left(\|\mathbf{x} - \mathbf{p}_i^t\|\right)\right) \tag{15}$$

where $\mathbf{E}^t(\mathbf{x})$ is interpreted as the energy field as a function of the distance from the focal particle. Interacting cells move along the gradient of the energy field, weighted by the interaction kernel as a function of particle-particle distance, and summed over all particles.

References

1. Chan, B. W.-C. Lenia-biology of artificial life. *arXiv preprint arXiv:1812.05433* (2018).
2. Chan, B. W.-C. Lenia and expanded universe. In *Artificial Life Conference Proceedings 32*, 221–229 (MIT Press One Rogers Street, Cambridge, MA 02142-1209, USA journals-info . . . , 2020).
3. Jain, S. & Shrestha, A. Capturing emerging complexity in lenia. *arXiv preprint arXiv:2305.09378* (2023).
4. Gardner, M. Mathematical games-the fantastic combinations of john conway's new solitaire game, life, 1970. *Scientific American, October* 120–123.
5. Davis, Q. T. & Bongard, J. Glaberish: generalizing the continuously-valued lenia framework to arbitrary life-like cellular automata. In *Artificial Life Conference Proceedings 34*, vol. 2022, 47 (MIT Press One Rogers Street, Cambridge, MA 02142-1209, USA journals-info . . . , 2022).
6. Plantec, E. *et al.* Flow lenia: Mass conservation for the study of virtual creatures in continuous cellular automata. *arXiv preprint arXiv:2212.07906* (2022).
7. Kawaguchi, T., Suzuki, R., Arita, T. & Chan, B. Introducing asymptotics to the state-updating rule in lenia. In *ALIFE 2022: The 2022 Conference on Artificial Life* (MIT Press, 2021).
8. Horibe, K., Suzuki, K., Horii, T. & Ishiguro, H. Exploring the adaptive behaviors of particle lenia: A perturbation-response analysis for computational agency. *arXiv preprint arXiv:2305.16706* (2023).
9. Kojima, H. & Ikegami, T. Implementation of lenia as a reaction-diffusion system. *arXiv preprint arXiv:2305.13784* (2023).
10. Gerlee, P. The model muddle: in search of tumor growth laws. *Cancer research* **73**, 2407–2411 (2013).
11. Benzekry, S. *et al.* Classical mathematical models for description and prediction of experimental tumor growth. *PLoS computational biology* **10**, e1003800 (2014).
12. Ghaffari Laleh, N. *et al.* Classical mathematical models for prediction of response to chemotherapy and immunotherapy. *PLoS computational biology* **18**, e1009822 (2022).
13. Baker, R. E. & Simpson, M. J. Correcting mean-field approximations for birth-death-movement processes. *Physical Review E* **82**, 041905 (2010).
14. West, J. & Newton, P. K. Cellular interactions constrain tumor growth. *Proceedings National Academy Sciences* **116**, 1918–1923 (2019).
15. Noble, R. *et al.* Spatial structure governs the mode of tumour evolution. *Nature Ecology & Evolution* **6**, 207–217 (2022).
16. Streck, A., Kaufmann, T. L. & Schwarz, R. F. Smith: spatially constrained stochastic model for simulation of intra-tumour heterogeneity. *Bioinformatics* **39**, btad102 (2023).
17. West, J., Schenck, R. O., Gatenbee, C., Robertson-Tessi, M. & Anderson, A. R. Normal tissue architecture determines the evolutionary course of cancer. *Nature communications* **12**, 2060 (2021).
18. Pérez-García, V. M. *et al.* Universal scaling laws rule explosive growth in human cancers. *Nature physics* **16**, 1232–1237 (2020).
19. Jiménez-Sánchez, J. *et al.* Evolutionary dynamics at the tumor edge reveal metabolic imaging biomarkers. *Proceedings National Academy Sciences* **118**, e2018110118 (2021).
20. Deutsch, A. & Dormann, S. *Mathematical modeling of biological pattern formation* (Springer, 2005).

21. Ryser, M. D., Min, B.-H., Siegmund, K. D. & Shibata, D. Spatial mutation patterns as markers of early colorectal tumor cell mobility. *Proceedings National Academy Sciences* **115**, 5774–5779 (2018).

22. Hoshino, T. *et al.* Pattern formation of skin cancers: Effects of cancer proliferation and hydrodynamic interactions. *Physical Review E* **99**, 032416 (2019).

23. Calcaterra, C. & Boldt, A. Existence of life in lenia. *arXiv preprint arXiv:2203.14390* (2022).

24. Maddalena, L. Analysis of an integro-differential system modeling tumor growth. *Applied Mathematics Computation* **245**, 152–157 (2014).

25. Jain, H. V. & Byrne, H. M. Qualitative analysis of an integro-differential equation model of periodic chemotherapy. *Applied Mathematics Letters* **25**, 2132–2136 (2012).

26. Greene, J. M. *et al.* Modeling intrinsic heterogeneity and growth of cancer cells. *Journal theoretical biology* **367**, 262–277 (2015).

27. Bekker, R. A. *et al.* Rethinking the immunotherapy numbers game. *Journal for immunotherapy cancer* **10** (2022).

28. Hamilton, P. T., Anholt, B. R. & Nelson, B. H. Tumour immunotherapy: lessons from predator–prey theory. *Nature Reviews Immunology* **22**, 765–775 (2022).

29. Kareva, I., Luddy, K. A., O'Farrelly, C., Gatenby, R. A. & Brown, J. S. Predator-prey in tumor-immune interactions: A wrong model or just an incomplete one? *Frontiers Immunology* **12**, 668221 (2021).

30. Brown, J. S., Cunningham, J. J. & Gatenby, R. A. Aggregation effects and population-based dynamics as a source of therapy resistance in cancer. *IEEE Transactions on Biomedical Engineering* **64**, 512–518 (2016).

31. Schiavo, M. L. Discrete kinetic cellular models of tumors immune system interactions. *Mathematical Models Methods Applied Sciences* **6**, 1187–1209 (1996).

32. Arlotti, L. & Lachowicz, M. Qualitative analysis of a nonlinear integrodifferential equation modeling tumor-host dynamics. *Mathematical computer modelling* **23**, 11–29 (1996).

33. Aylaj, B. Qualitative analysis and simulation of a nonlinear integro-differential system modeling tumor-immune cells competition. *International Journal Biomathematics* **11**, 1850104 (2018).

34. Kolev, M. Mathematical modelling of the competition between tumors and immune system considering the role of the antibodies. *Mathematical Computer Modelling* **37**, 1143–1152 (2003).

35. Lachowicz, M. & Quartarone, A. A general framework for modeling tumor-immune system competition at the mesoscopic level. *Applied Mathematics Letters* **25**, 2118–2122 (2012).

36. Alfonso, J. C. *et al.* Tumor-immune ecosystem dynamics define an individual radiation immune score to predict pan-cancer radiocurability. *Neoplasia* **23**, 1110–1122 (2021).

37. Abhilash, A., Baker, B., Trappmann, B., Chen, C. & Shenoy, V. Remodeling of fibrous extracellular matrices by contractile cells: predictions from discrete fiber network simulations. *Biophys* **107**, 1829–1840 (2014).

38. Suveges, S., Chamseddine, I., Rejniak, K. A., Eftimie, R. & Trucu, D. Collective cell migration in a fibrous environment: A hybrid multiscale modelling approach. *Frontiers Applied Mathematics Statistics* **7**, DOI: 10.3389/fams.2021.680029 (2021).

39. Sabeh, F., Shimizu-Hirota, R. & Weiss, S. J. Protease-dependent versus-independent cancer cell invasion programs: three-dimensional amoeboid movement revisited. *Journal Cell Biology* **185**, 11–19 (2009).

40. Sage, D. Orientationj: A series of imagej plugins for directional image analysis. *Biomedical Image Group at EPFL, Switzerland* (2020).

41. Saito, T. *et al.* Aberrant collagen cross-linking in human oral squamous cell carcinoma. *Journal dental research* **98**, 517–525 (2019).

42. Lennard-Jones, J. E. Cohesion. *Proceedings Physical Society* **43**, 461 (1931).

43. Franco-Barraza, J., Beacham, D. A., Amatangelo, M. D. & Cukierman, E. Preparation of extracellular matrices produced by cultured and primary fibroblasts. *Current protocols cell biology* **71**, 10–9 (2016).

44. Gallaher, J. A., Enriquez-Navas, P. M., Luddy, K. A., Gatenby, R. A. & Anderson, A. R. Spatial heterogeneity and evolutionary dynamics modulate time to recurrence in continuous and adaptive cancer therapies. *Cancer Research* **78**, 2127–2139 (2018).

45. Strobl, M. A. R. *et al.* Turnover modulates the need for a cost of resistance in adaptive therapy. *BioRxiv* (2020).

46. Dénes, A., Marzban, S. & Röst, G. Global analysis of a cancer model with drug resistance due to lamarckian induction and microvesicle transfer. *Journal Theoretical Biology* **527**, 110812, DOI: https://doi.org/10.1016/j.jtbi.2021.110812 (2021).

47. Hamis, S. *et al.* Spatial cumulant models enable spatially informed treatment strategies and analysis of local interactions in cancer systems. *Journal Mathematical Biology* **86**, 68 (2023).

48. Nowak, M. A. *Evolutionary Dynamics* (Harvard University Press, 2006).

49. You, L. *et al.* Spatial vs. non-spatial eco-evolutionary dynamics in a tumor growth model. *Journal Theoretical Biology* **435**, 78–97 (2017).

A Lenia artificial life virtual creatures identified through interactive evolutionary computation

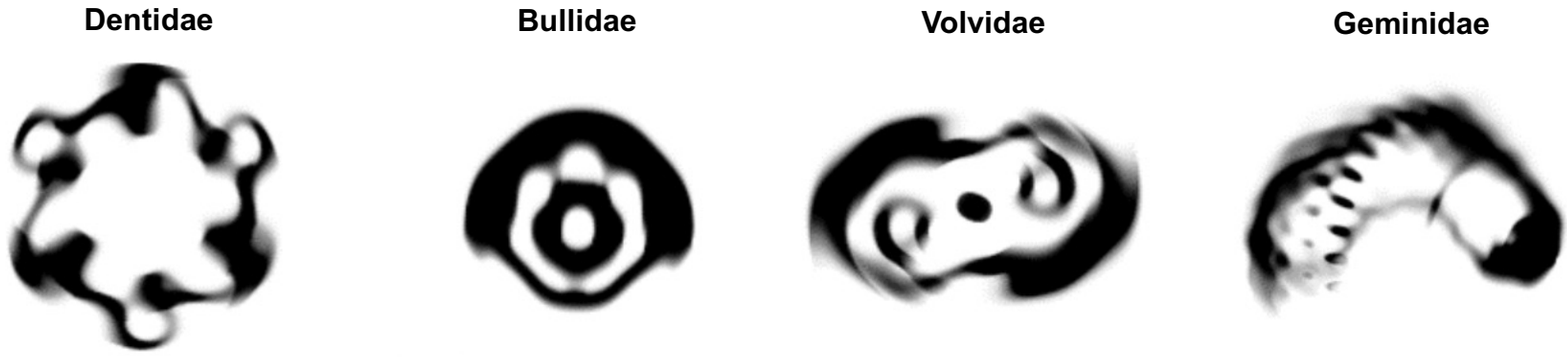

B Lenia Characteristics

- morphogenesis
- homeostasis
- self-direction / motility
- self-replication
- growth / development
- stimuli response
- evolvability
- adaptation

C Growth dynamics, G(u)

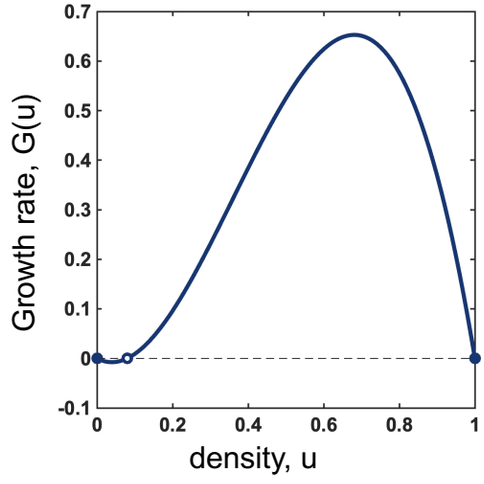

D Interaction kernel function

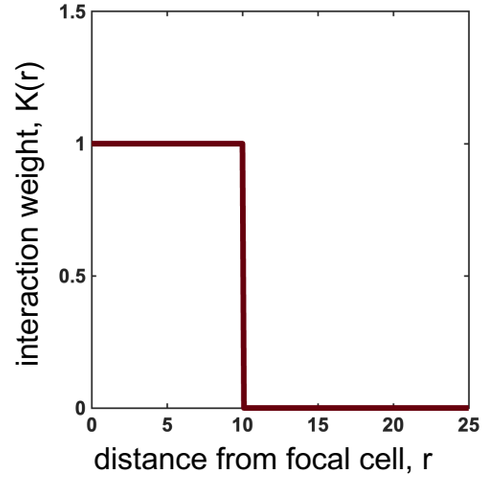

E Cell density, $\mathbf{A}(\mathbf{x})$

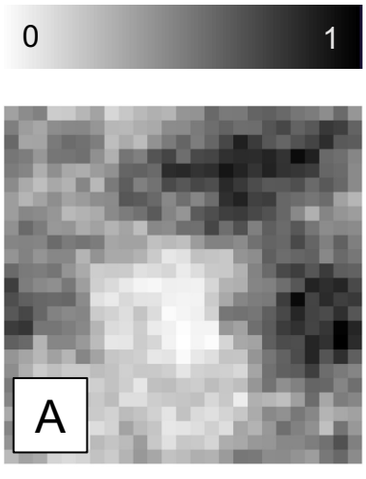

F Interaction kernel, $\mathbf{K}(\mathbf{x})$

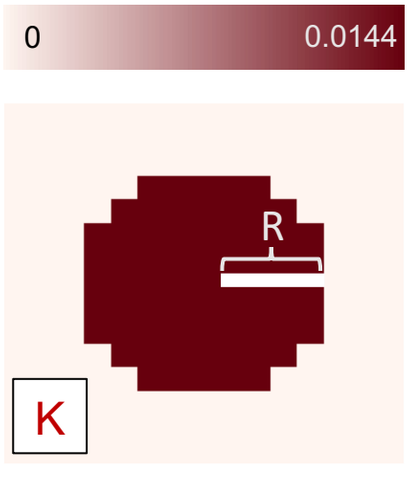

G Density potential, $\mathbf{U}(\mathbf{x})$

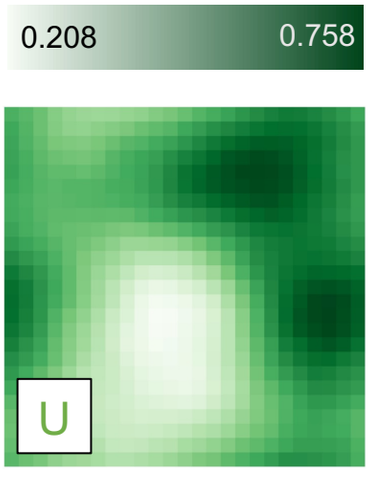

H Growth field, $\mathbf{G}(\mathbf{x})$

I Lenia update rule

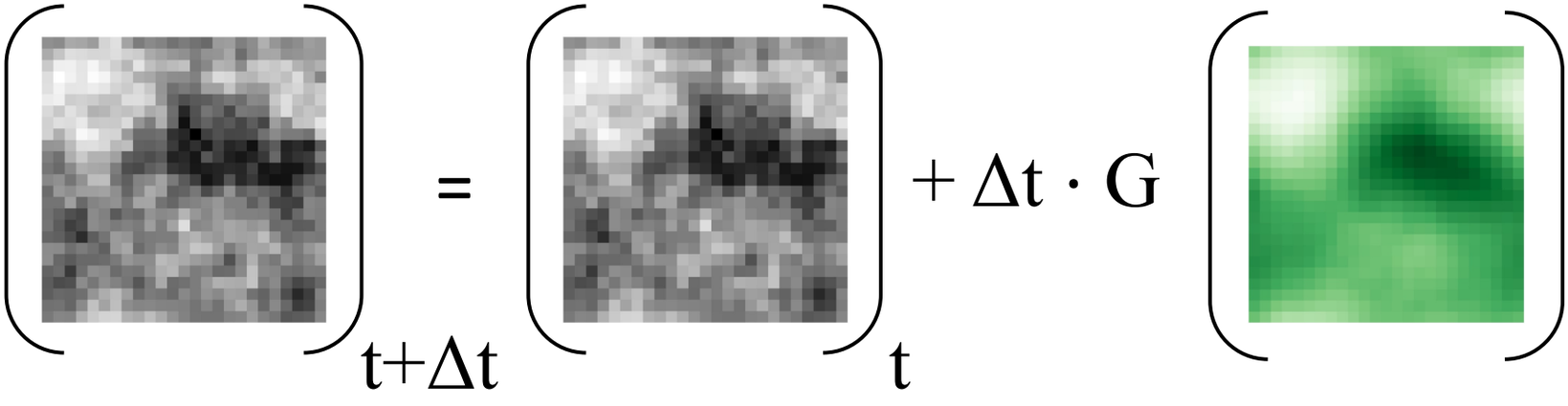

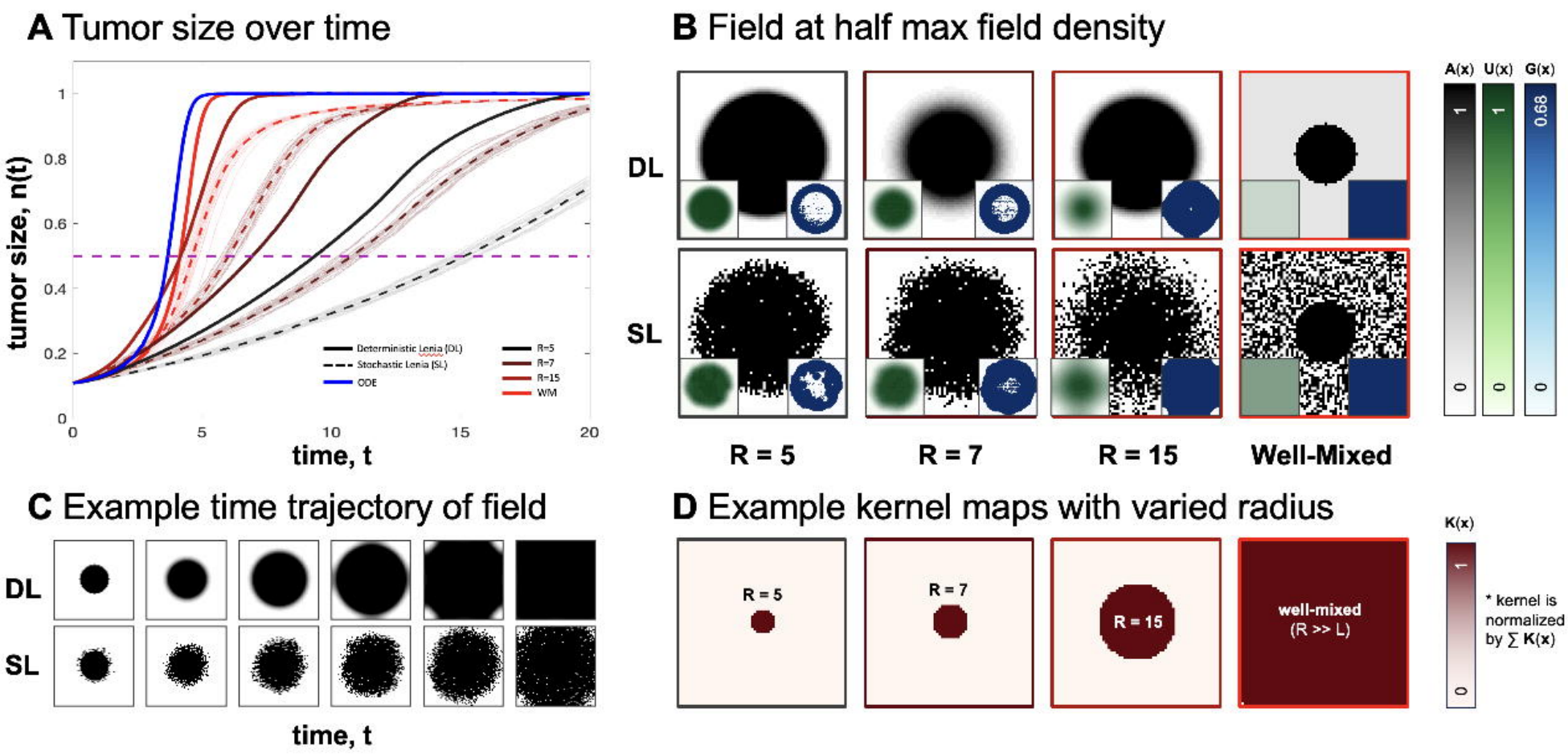
A Tumor size over time
tumor size, n(t)
time, t
Deterministic Lenia (DL)
Stochastic Lenia (SL)
ODE
R=5
R=7
R=15
WM
B Field at half max field density
DL
SL
R = 5
R = 7
R = 15
Well-Mixed
A(x)
U(x)
G(x)
C Example time trajectory of field
DL
SL
time, t
D Example kernel maps with varied radius
R = 5
R = 7
R = 15
well-mixed
(R >> L)
K(x)
* kernel is normalized by ∑ K(x)

Short-range interaction kernels are robust to Allee effects

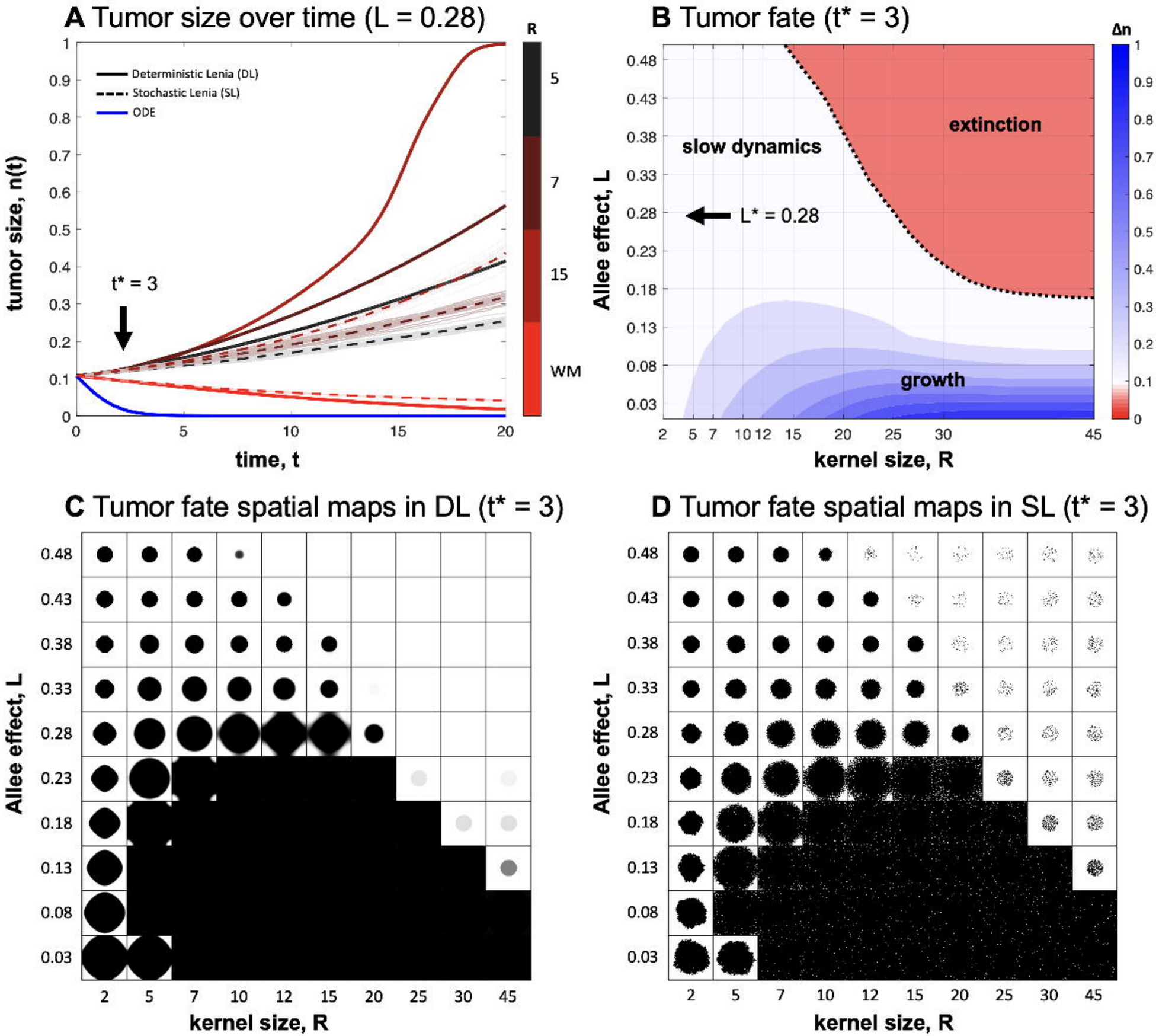

A. Tumor-immune predator-prey model schematic

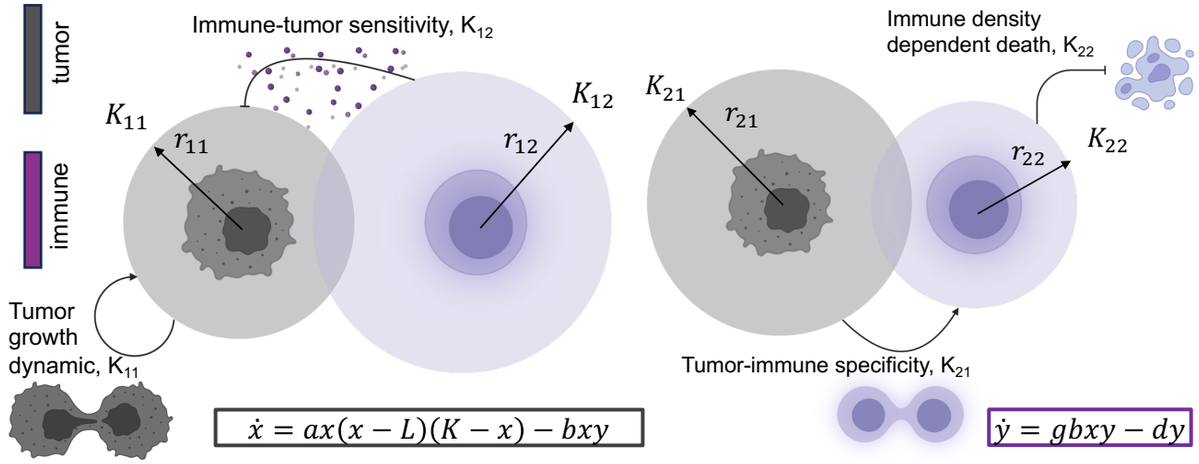

B. Increased tumor-immune <u>sensitivity</u> K_{12} decreases TTR & IPV

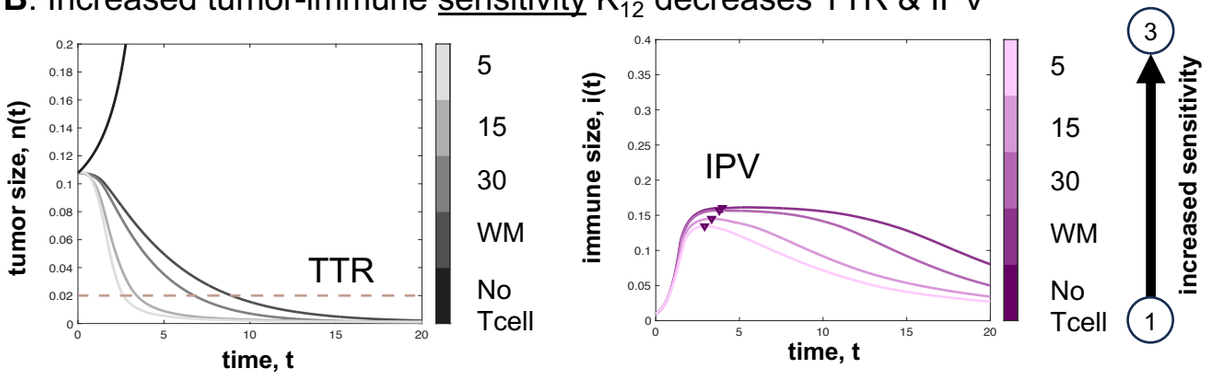

C. Increased tumor-immune <u>specificity</u> K_{21} decreases TTR & IPV

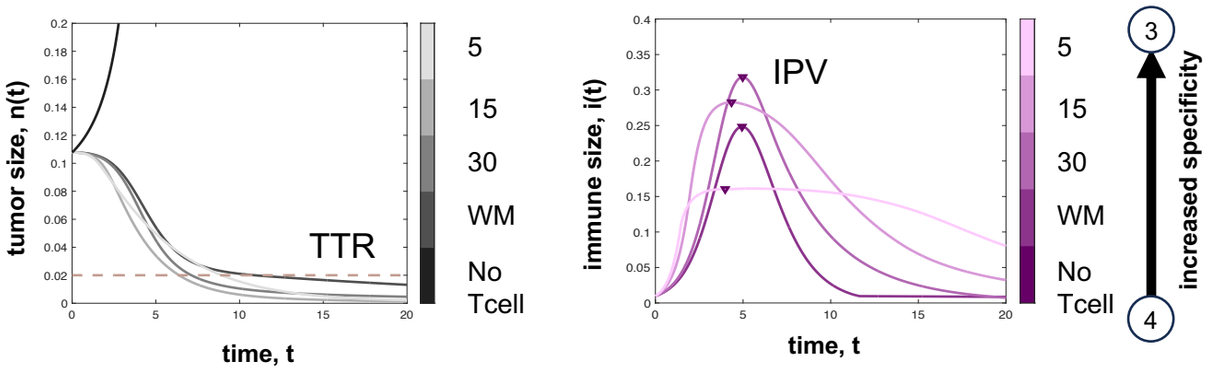

D. High sensitivity and specificity minimize time to tumor regression

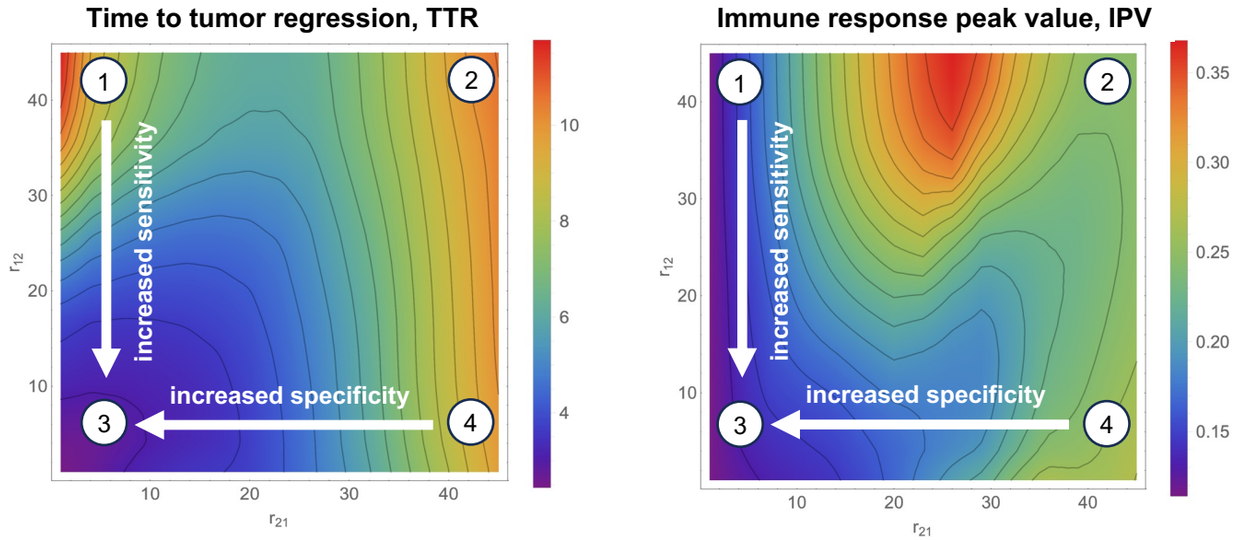

E. The effect of sensitivity and specificity on spatial assortment of immune-tumor

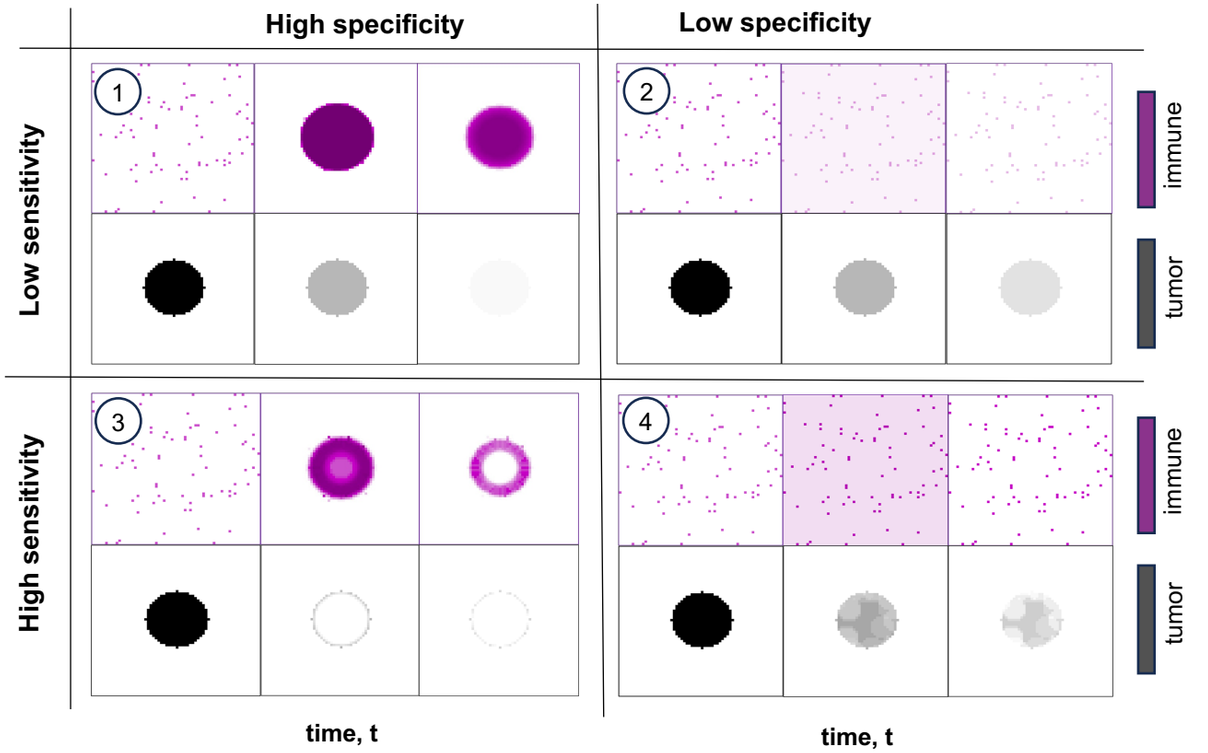

A Image analysis to computational model pipeline

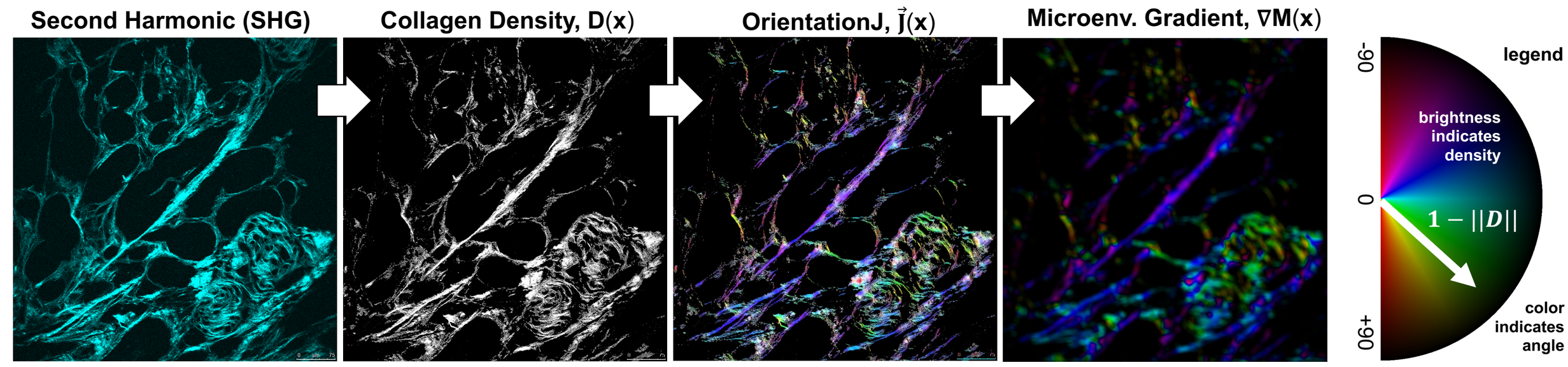

B Quantification of collagen alignment in HNSCC by disease stage

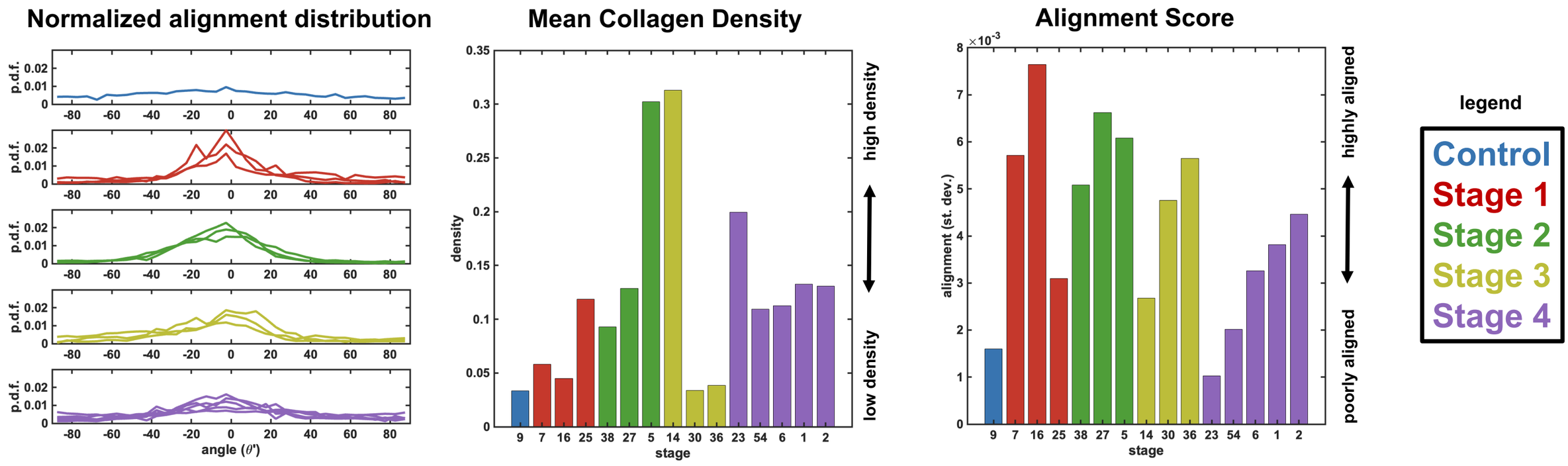

C Immune trafficking in head and neck squamous cell carcinoma by stage

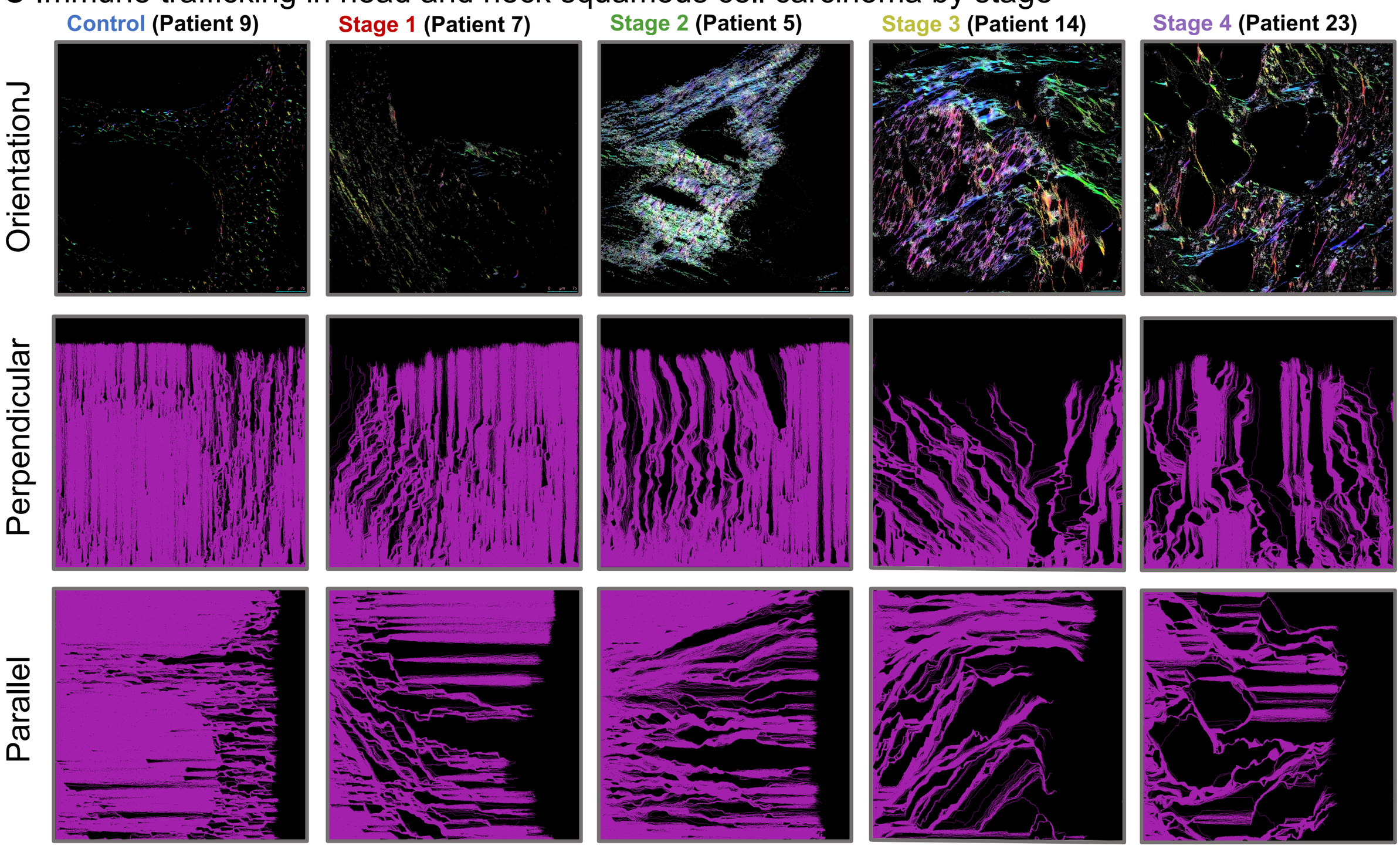

D Immune infiltration

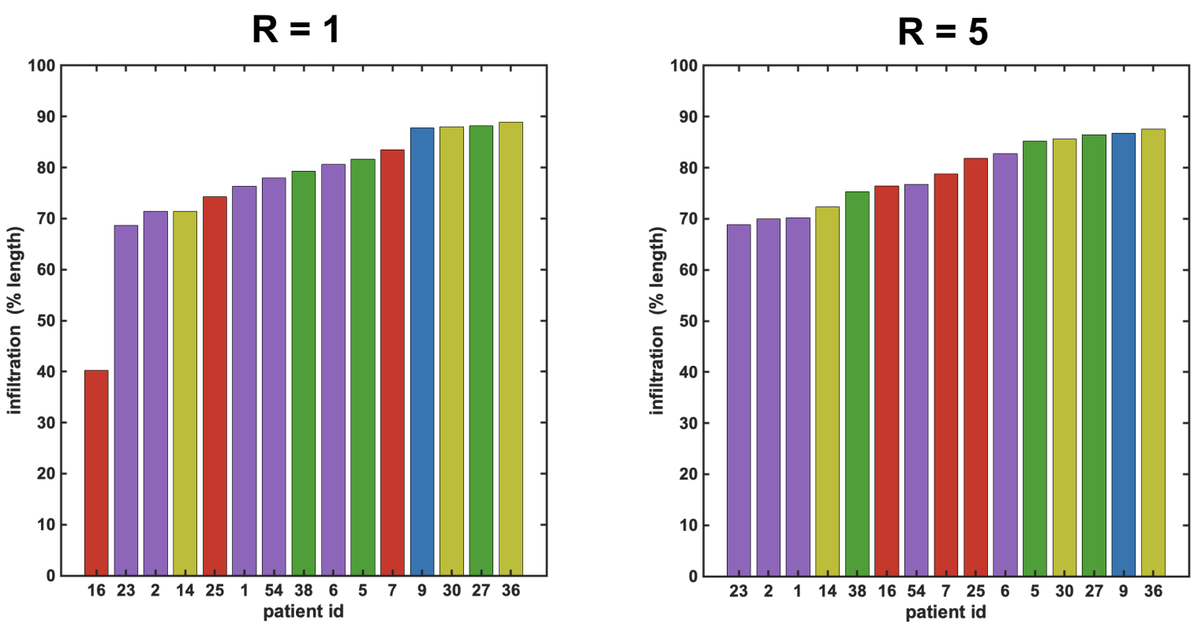
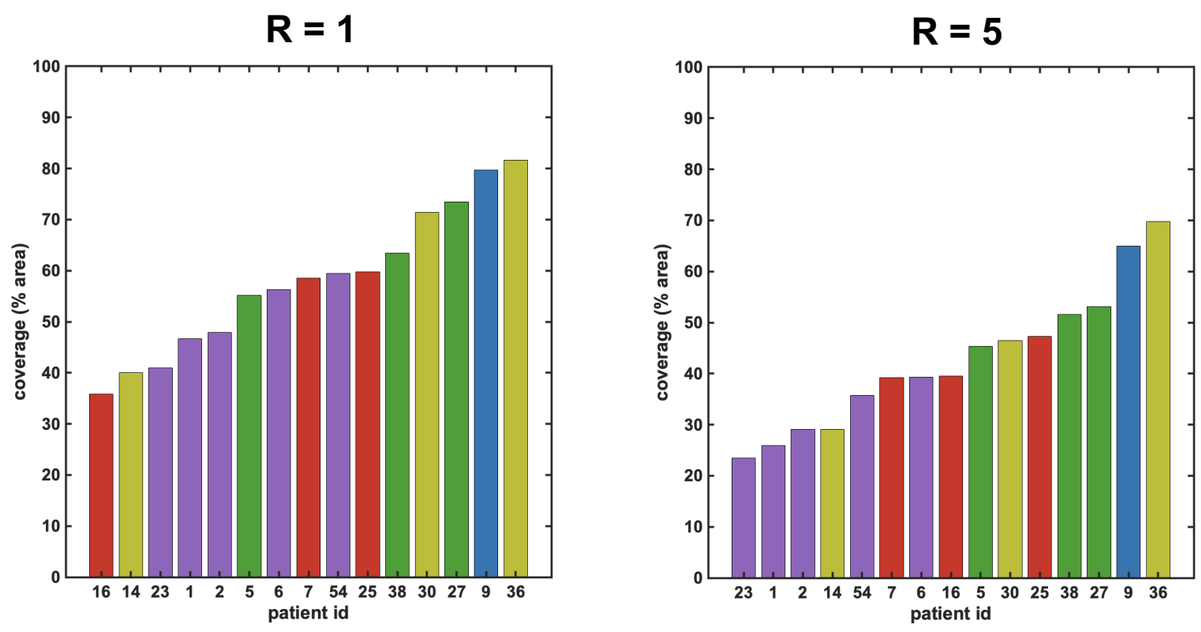
E Immune coverage